



OPEN

Parameter identification of Johnson–Cook constitutive model based on genetic algorithm and simulation analysis for 304 stainless steel

Xinyang Jiang¹, Jinfu Ding¹, Chengwu Wang^{1,2✉}, E Shiju¹, Ling Hong^{3✉}, Weifeng Yao⁴, Huadong Wang¹, Chongqiu Zhou¹ & Wei Yu⁵

Addressing the significant discrepancy between actual experimental cutting force and its predicted values derived from traditional constitutive model parameter identification methods, a reverse identification research of the Johnson–Cook (J-C) constitutive model for 304 stainless steel was conducted via genetic algorithm. Considering actual cutting zone and the influence of feed motion on the rake (flank) angle, an unequal division shear zone model was established to implement the theoretical calculation for shear zone stress. Through cutting experiments, the spindle speed was negatively correlated with the cutting force at first, and then became positively correlated; The empirical formula (EXP model) for turning force was corrected, revealing that the EXP model was unable to provide optimal predicted values for cutting force. The influence of the J-C constitutive parameter C on the cutting morphology was firstly investigated through simulation analysis, and determined an appropriate value for C , then obtained the precise values for the other four constitutive parameters by genetic algorithm. Moreover, the simulated values of cutting force in JC1 model (obtained from the Split Hopkinson Pressure Bar test) and JCM model (the improved model using genetic algorithm) were obtained by three-dimensional (3-D) simulation via FEM software. The results indicated that, the maximum error between actual experimental cutting force and its simulated values (by JCM model) was 14.8%, with an average error of 6.38%. These results outperformed the JC1 and EXP models, suggesting that the JCM model identified via genetic algorithm was more reliable.

Owing to excellent performance, such as high thermal stability, corrosion resistance, and high-temperature resistance, 304 stainless steel (0Cr19Ni9) is widely applied in industries like chemical engineering, aerospace, medical equipment, and food processing¹. The hardness and strength of 304 stainless steel are relatively low, while its plasticity and toughness are relatively high. Moreover, its thermal conductivity is inferior, leading to high cutting temperature, severe work hardening and more machining force, which gave rise to the production of continuous and non-breakable chips². These can easily damage the surface of the workpiece³, and seriously affect its surface accuracy and decrease the durability of the cutting tool, ultimately reducing processing efficiency and quality^{4,5}. Therefore, the cutting force continues to be one of the essential elements in the investigation of the machinability of 304 stainless steel.

To accurately depict the mechanism of cutting force formation, it is necessary to analyze the shear zone at the interaction between tool tip and workpiece. Oxley⁶ was the first to propose the parallel shear zone model, suggesting that the shear zones were parallel and bisected by primary shear plane. However, Astakhov⁷ and Tounsi et al.⁸ found after experimental researches that the shear zones were not bisected, although they were parallel.

¹College of Engineering, Zhejiang Normal University, Jinhua 321004, China. ²Key Laboratory of Urban Rail Transit Intelligent Operation and Maintenance Technology & Equipment of Zhejiang Province, Zhejiang Normal University, Jinhua 321004, China. ³Zhejiang Shuohe Robot Technology Co., Ltd, Jinhua 321000, China. ⁴College of Mechanical and Electrical Engineering, Shaoxing University, Shaoxing 321017, China. ⁵College of Electrical and Information Engineering, Quzhou University, Quzhou 324000, China. ✉email: cwuwang@126.com; hongling@seokho.cn

Based on the unequal division shear zone model, Zhou et al.⁹ established a temperature distribution model. After comparative analysis, their predicted results indicated that the present model was in good agreement with the actual experimental results. Therefore, to delve into the stress–strain relationship of materials, researchers have established various constitutive models, such as the Bonder-Partom model¹⁰, Johnson–Cook (J–C) model¹¹ and Zerillo-Armstrong model¹². Among them, the J–C model is most widely applied. Its main parameters are: the initial yield stress A , the material strain strengthening coefficient B , the strain rate sensitivity C , the thermal softening index m , and the hardening index n .

Typically, the applicable strain rate range in Split Hopkinson Pressure Bar (SHPB) experiments lies between 10^3 s^{-1} and 10^4 s^{-1} , while in quasi-static tests, it spans from 10^{-4} s^{-1} to 10^{-1} s^{-1} . However, during machining processes, the strain rate of the material can reach up to 10^5 s^{-1} ¹³. This indicates that the constitutive parameters derived from SHPB or quasi-static tests do not accurately represent the stress–strain relationship of materials under cutting conditions. Therefore, many scholars have conducted a series of studies on constitutive models and their parameters. Hou et al.¹⁴ studied the plastic response of hot-extruded Mg-10Gd-2Y-0.5Zr alloy under both quasi-static and wide range temperature, finally obtained an improved J–C model. Meng et al.¹⁵ obtained two J–C constitutive models for ADC12 alloy using split Hopkinson pressure bar (SHPB) experiments. The comparison between simulated flow stress and experimental data suggested that the refined J–C constitutive model offered a more precise prediction of flow stress under conditions of high strain rates and elevated temperatures. Chen et al.¹⁶ identified J–C constitutive parameters (C and m) by conducting two-dimensional (2-D) cutting force simulations via orthogonal cutting experiments for Al6063 aluminum material, and subsequently obtained other constitutive parameters (A , B , and n) by compression tests. It was found that this method was much more economical and could obtain more accurate simulated cutting forces, by comparison with the traditional SHPB experiment. Shen et al.¹⁷ acquired the J–C constitutive model of TC17 titanium alloy through SHPB experiment, and also obtained another J–C constitutive model via parameter identification. By contrast, the model parameters obtained by parameter identification were more suitable for the prediction of cutting forces.

Additionally, due to the inability of constitutive parameters to accurately characterize the stress–strain relationship under specific operational conditions, many scholars have conducted studies on the numerical optimization of constitutive parameters. Nguyen and Hosseini¹⁸ combined J–C flow stress model with Oxley machining model to calculate the cutting forces during milling, finally obtained the J–C constitutive parameters (C , m) and thermal coefficients (η , ψ) of AISI 4340 hardened steel. They found that the results of predicted cutting forces revealed great consistency with its experimental value. Zhou et al.¹⁹ realized the least squares identification of J–C constitutive parameters and improved the prediction accuracy of cutting force by modeling and simulation for H13 steel and Ti-6Al-4 V titanium alloy. Zou et al.¹³ implemented the reverse identification of J–C parameters of 304 stainless steel by adopting the minimum error between experimental value and simulated value of cutting force as the objective function of genetic algorithm. They also established the three-dimensional (3-D) model as the initial model for finite element iteration, compared the experimental cutting force, chip morphology, and residual stress. It was found that the constitutive parameters A and B had a much greater impact on cutting force than parameters C , m , and n during simulation. According to hot tensile test, neural networks and genetic algorithm, Yao et al.²⁰ obtained the constitutive parameters of AA6061 aluminum alloy via reverse identification. It was reported that the accuracy of hybrid identification method was better than single optimized algorithm, since the initial population of genetic algorithm was optimized by neural network.

The objective of this study is to efficiently obtain more accurate constitutive parameters via genetic algorithm. Firstly, considering the influence of tool parameters on cutting zone and the impact of feed motion on the rake (flank) angle, an unequal division shear zone model was established. Then, the effect of the constitutive parameter C on chip morphology was figured out via finite element simulation. Furthermore, turning experiments were conducted to analyze the effects of experimental parameters (spindle speed n , feed rate f , and cutting depth a_p) on cutting force, and J–C constitutive model parameters were identified via genetic algorithm. Finally, the feasibility of the reverse identification method and the reliability as well as accuracy of constitutive model were verified by comparing the predicted results of empirical formula with simulation results.

Cutting zone modeling

Figure 1 exhibits the scheme of cutting zone during feed motion. During one complete revolution of the spindle, the tool progresses from position I to position II. The cutting thickness a is the dimension of the cutting layer measured perpendicularly to the main cutting edge within the base, representing the load on the cutting edge per unit length; The cutting width b refers to the projection of working length of the main cutting edge on base plane. The relationships between cutting thickness a , cutting width b , feed rate f (The distance S , which the tool travels as the workpiece makes one full rotation, is numerically equivalent to the feed rate f), and cutting depth a_p are as follows:

$$a = S \sin K_r \quad (1)$$

$$b = \frac{a_p}{\sin K_r} \quad (2)$$

where, K_r refers to the tool cutting edge angle.

Theoretical cutting zone S_A was calculated through cutting thickness a and cutting width b :

$$S_A = a \cdot b = S \cdot a_p \quad (3)$$

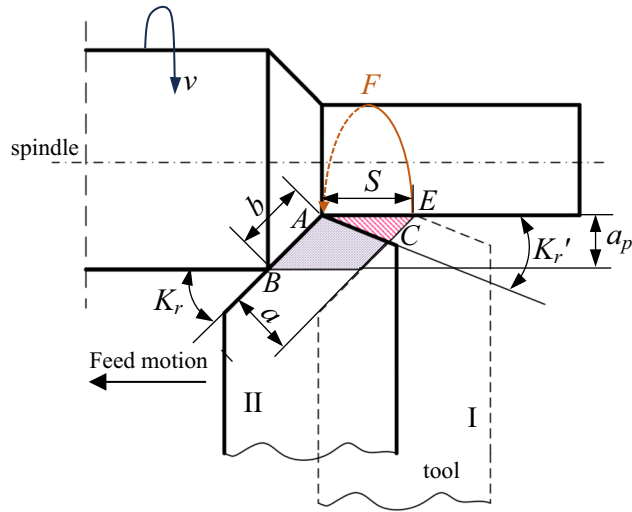


Fig. 1. Cutting thickness and cutting width.

Due to the presence of end cutting edge angle K_r' on turning tool, and the trajectory of tool tip following an arc EFA along the outer circumference of the workpiece, a small residual zone (see $S_{\Delta ACE}$ shown in Fig. 1) is left on the machined workpiece surface. Therefore, the actual cutting zone could be obtained via subtracting the theoretical cutting zone S_A by the residual zone $S_{\Delta ACE}$:

$$\begin{cases} \frac{S}{\sin(\pi - K_r - K_r')} = \frac{AC}{\sin K_r} = \frac{CE}{\sin K_r'} \\ S_{ACE} = \frac{1}{2} \sin(\pi - K_r - K_r') AC CE \\ = \frac{1}{2} \cdot \frac{S^2 \sin K_r \sin K_r'}{\sin(\pi - K_r - K_r')} \\ S_{A'} = S_A - S_{ACE} = Sa_p - \frac{1}{2} \frac{S^2 \sin K_r \sin K_r'}{\sin(\pi - K_r - K_r')} \end{cases} \quad (4)$$

As shown in Fig. 2, due to the feed motion of lathe machining, the actual cutting surface is a helical surface with a helix μ , which will affect the rake angle γ_0 and flank angle α_0 :

$$\tan \mu = \frac{S}{\pi d} \quad (5)$$

where, d is workpiece diameter (mm). Then, the actual rake angle γ_0' and flank angle α_0' are:

$$\gamma_0' = \gamma_0 + \mu \quad (6)$$

$$\alpha_0' = \alpha_0 - \mu \quad (7)$$

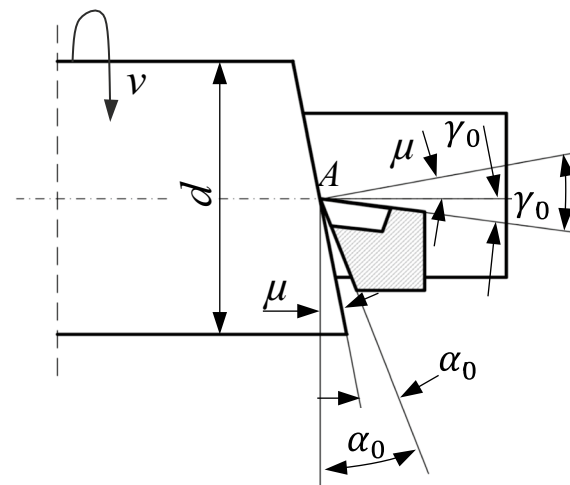


Fig. 2. The influence of feed motion on rake and flank angles.

Establishment of unequal division shear zone model and constitutive equation

As shown in Fig. 3, a shear zone model of the workpiece during the turning process has been constructed. Longitudinal turning is considered as oblique cutting (see Fig. 3a) due to the existence of the inclination angle λ_s . The shear zone in the equivalent plane P_n of orthogonal cutting is shown in Fig. 3b) after equivalently converting oblique cutting to orthogonal cutting^{21,22}.

The projections of cutting force F_y , main cutting force F_z , and cutting speed v in the equivalent plane P_n are denoted as $F_{y'}$, $F_{z'}$, and v' , respectively. Their relationships are as follows:

$$\begin{cases} F_{y'} = F_y \\ F_{z'} = F_x \cos \lambda_s \\ v' = v \cos \lambda_s \end{cases} \quad (8)$$

It is reported in literature²³ that the shear zone of cutting deformation was located at the contacting point of tool tip and workpiece, and the primary shear zone was very narrow with high strain rate. Oxley⁶ thought that the primary shear plane bisected the primary shear zone and was parallel to the initial shear plane and final shear plane. Astakhov⁷ believed that the speed of machining chips within the shear zone varied, and divided it into narrow and wide zones. Tounsi⁸ continued Astakhov's theory and defined the thickness of the wide zone as k times the overall thickness of the primary shear band. Li et al.²⁴ employed an unequal division shear zone model to predict the cutting forces during orthogonal cutting, and their predicted results were in good agreement with the experimental outcomes. Therefore, this study established an unequal division shear zone model (see Fig. 3b).

As shown in Fig. 3b), the shear velocity v_s is parallel to the primary shear plane AA_1 , while the chip velocity v_c is parallel to the rake face of tool. The primary shear plane AA_1 is parallel with the initial shear plane PQ and the final shear plane MN , dividing the shear zone into two unequal parts. The distance from PQ to MN is h , and the distance from AA_1 to PQ is k times h . The relationship between the shear zone unequal division coefficient k , the shear angle ϕ and the actual rake angle γ_0' is obtained from literature⁸:

$$k = \frac{1}{2} + \frac{\cos(2\phi - \gamma_0')}{2\cos(\gamma_0')} \quad (9)$$

The approximation formula of shear angle ϕ by Lee and Shaffer gives:

$$\phi = \frac{\pi}{4} - (\beta - \gamma_0') \quad (10)$$

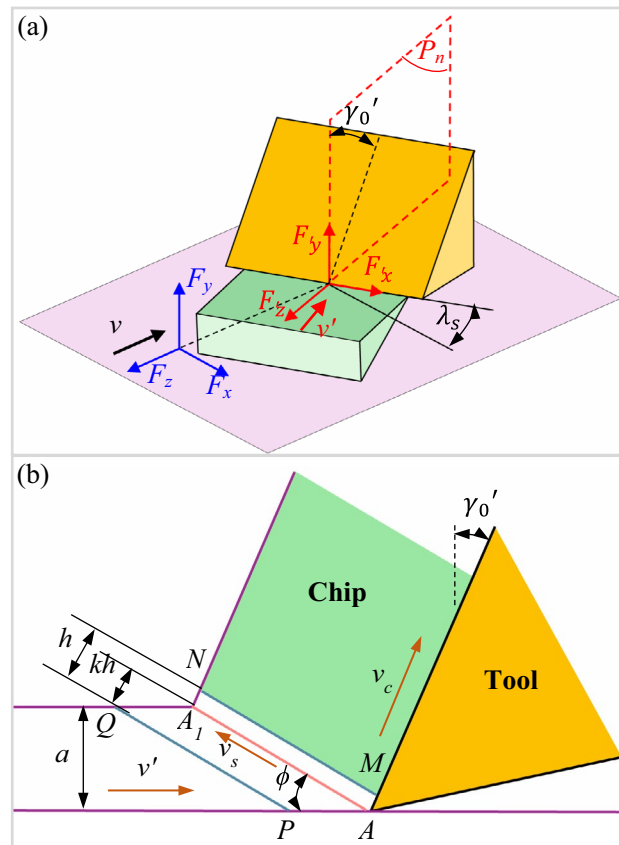


Fig. 3. (a) Oblique cutting model; (b) The unequal division shear zone model in the equivalent plane P_n ²¹.

The friction angle β can be obtained from the following formula:

$$\beta = \arctan\left(\frac{F_{y'}}{F_{z'}}\right) + \gamma_0' \quad (11)$$

The strain ε_{AB} of the primary shear plane:

$$\varepsilon_{AB} = k \left[\frac{\cos(\gamma_0')}{\sqrt{3}\cos(\phi - \gamma_0')\sin\phi} \right] \quad (12)$$

The strain rate $\dot{\varepsilon}_{AB}$ of the primary shear plane:

$$\dot{\varepsilon}_{AB} = \frac{2v' \cdot \cos(\gamma_0')}{\sqrt{3} \times 0.5f \cos(\phi - \gamma_0')} \quad (13)$$

The shear stress τ_{AB} of the primary shear plane:

$$\tau_{AB} = \frac{\sin\phi}{S_{A'}} [F_{z'} \cos\phi - F_{y'} \sin\phi] \quad (14)$$

The temperature T_{AB} of the primary shear plane:

$$T_{AB} = T_r + \left[\frac{k\cos\gamma_0'}{\rho C_p \sin\phi \cos(\phi - \gamma_0')} \right] \left(\frac{2\tau_{AB} + \tau_0}{3} \right) \quad (15)$$

where, ρ refers to the material density, C_p represents the specific heat capacity. Through the relationship between τ_{AB} and principal stress σ_{AB} , then $\sigma_{AB} = \sqrt{3}\tau_{AB}$, $\tau_0 = \frac{\sigma_e}{\sqrt{3}}$, and σ_e refers to the elastic limit stress.

The constitutive model²⁵ is a general model that describes all the fundamental information during material deformation process. It can depict the relationships among various thermomechanical parameters induced by mechanical-thermal coupling in deformation, such as stress and strain, strain rate and temperature.

In this study, the Johnson–Cook constitutive model is used to describe the relationship of stress and strain. Its expression is as follow:

$$\sigma = (A + B\varepsilon^n) \left[1 + \text{Cln}\left(\frac{\dot{\varepsilon}}{\dot{\varepsilon}_0}\right) \right] \left[1 - \left(\frac{T - T_r}{T_m - T_r}\right)^m \right] \quad (16)$$

where, A represents the initial yield stress, MPa; B is the material strain strengthening coefficient, MPa; C represents the strain rate sensitivity; m expresses the thermal softening index; n is the hardening index exponent; σ is the flow stress, MPa; ε refers to the equivalent plastic strain; $\dot{\varepsilon}$ denotes the equivalent strain rate, s^{-1} ; $\dot{\varepsilon}_0$ is the reference strain rate of 304 stainless steel material, s^{-1} ; T expresses the material deformation temperature, °C; T_m is the melting temperature, °C; T_r is the room temperature, °C.

According to the least squares principle, the fitness function of genetic algorithm is obtained as⁸:

$$(A, B, n, C, m) = k_1 \left(\sum_{i=1}^N \left[\frac{A + B\varepsilon_{AB}^n(i)}{\sigma_{AB}} \left(1 + \text{Cln}\left(\frac{\dot{\varepsilon}_{AB}(i)}{\dot{\varepsilon}_0}\right) \right) \left(1 - \left(\frac{T_{AB}(i) - T_r}{T_m - T_r}\right)^m \right) - 1 \right]^2 \right) \quad (17)$$

N represents the number of experimental groups, i expresses the experimental sequence number, and k_1 refers to a proportionality constant value - 1.

Turning experiments and result analysis

The cutting system used in this study is shown in Fig. 4. The material employed in cutting experiment was 304 stainless steel rod, with a diameter of 40 mm and a length of 400 mm. The cutting equipment used was ordinary lathe (CA6140 400 × 1000), assembled with a turning tool holder (MWLNR2020K08), made of 40CR-42CRMO, with tool cutting edge angle K_r of 95°, end cutting edge angle K_r' of 5° and a dimension of 20 × 125 × 20 mm. The model of turning insert was WNMG080408-SM, made of WM3125, with corner radius of 0.8 mm, rake angle γ_0 of 6° and inclination angle λ_s of 6°.

In this experiment, the cutting forces were measured with a force measuring system, which include a Kistler dynamometer type 9257B, charge amplifier type 5080A, 5697A data acquisition system, and computer with the DynoWare software, as shown in Fig. 4d. In actual turning process on ordinary lathe, the lathe spindle speed (n) remained constant, whereas without the help of computer numerical control, the cutting speed (v) would vary with the change of rod diameter. Therefore, the spindle speed rather than cutting speed was focused through experimental discussing and analyzing. As shown in Table 1, the spindle speed (n), cutting depth (a_p), and feed rate (f) were chosen as experimental parameters. As shown in Table 2, a three-factor three-level cutting experiment was designed with a total of 27 groups experimental data, additionally, the cutting speed is also provided. Table 3 and Fig. 5 were obtained by range analysis of F_z . Delta represents the extent to which the parameter affects the cutting force F_z . The larger the Delta value, the greater its impact, resulting in a smaller assigned Rank.

According to the data presented in Table 3, it is evident that the cutting depth (Delta = 77.82, Rank = 1) exerts the most significant influence on F_z . Subsequently, the feed rate (Delta = 48.05, Rank = 2) follows in terms of impact, and lastly, the spindle speed (Delta = 14.4, Rank = 3). Based on the findings presented in Fig. 5, the

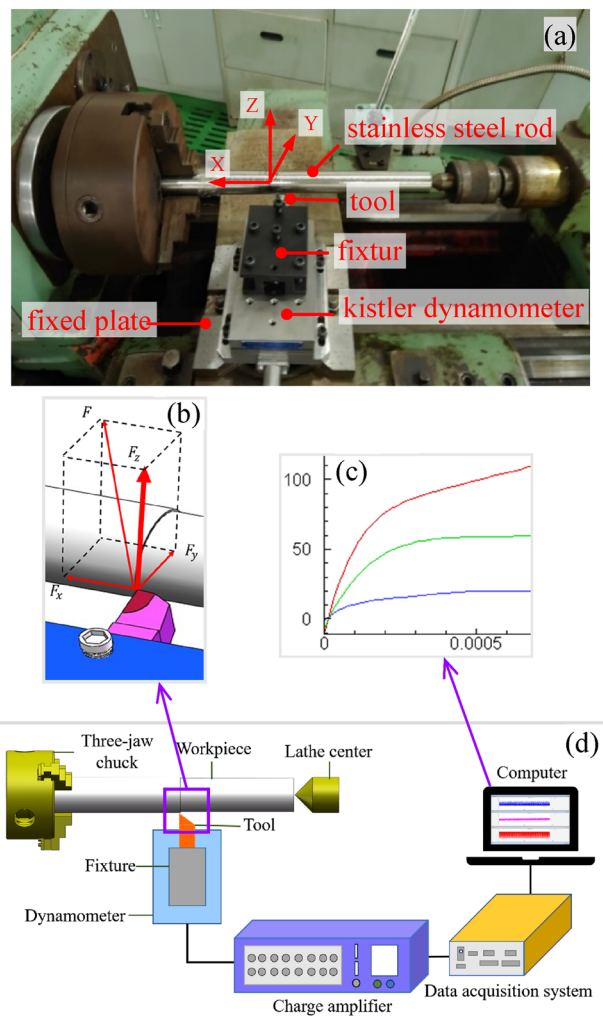


Fig. 4. Turning test devices.

Level	spindle speed n (r/min)	cutting depth a_p (mm)	feed rate f (mm/r)
1	400	0.1	0.08
2	560	0.2	0.12
3	710	0.3	0.15

Table 1. Experimental parameters.

cutting depth and feed rate have a positive correlation with the cutting force F_z . Equation (1)–(4) demonstrate that augmenting the cutting depth and feed rate will have an impact on the cutting width and thickness, thereby resulting in an expansion of the cutting zone. During the initial stages of cutting experiments, cutting force measurements were conducted at spindle speeds of 560 and 710 r/min. The impact of the workpiece diameter on the cutting speed proved to be minimal. In the range of 560 to 710 r/min, as the spindle speed increases, the cutting speed also increases, leading to a greater plastic deformation of the workpiece within a given time frame. Consequently, the spindle speed has a positive correlation with the cutting force F_z . While, at a spindle speed of 400 r/min, significant workpiece wear was observed. Results in a decrease in cutting speed and an increase in the rake angle during the feed motion, led to a reduction in both shear surface strain and strain rate. Consequently, the spindle speed between 400 and 560 r/min was inversely correlated with the cutting force F_z .

Genetic algorithm identification of J–C model constitutive parameters

Genetic algorithm (GA) is a method for searching the optimal solution by simulating the natural evolutionary process. Renowned for its robust global search capability, GA has been applied in parameter identification. Zhou et al. utilized the genetic algorithm to identify and improve J–C constitutive model, achieving higher precision in

Experiment number	n (r/min)	D (mm)	v (m/min)	f (mm/r)	a_p (mm)	F_y (N)	F_z (N)
1	400	31.8	39.94	0.08	0.1	39.02	62.46
2	400	31.6	39.69	0.12	0.1	43.84	75.57
3	400	29.4	36.93	0.15	0.1	52.32	94.43
4	400	26.8	33.66	0.08	0.2	51.25	87.39
5	400	31.4	39.44	0.12	0.2	72.78	121.92
6	400	29.8	37.43	0.15	0.2	84.65	145.89
7	400	32.8	41.20	0.08	0.3	65.31	112.80
8	400	27.5	34.54	0.12	0.3	85.59	168.92
9	400	28.7	36.05	0.15	0.3	97.96	174.13
10	560	39.0	68.58	0.08	0.1	16.54	47.99
11	560	23.8	41.85	0.12	0.1	47.27	59.09
12	560	38.6	67.87	0.15	0.1	55.69	86.15
13	560	25.0	43.96	0.08	0.2	56.40	96.42
14	560	36.8	64.71	0.12	0.2	72.02	104.18
15	560	38.4	67.52	0.15	0.2	89.05	116.78
16	560	40.0	70.34	0.08	0.3	47.44	110.23
17	560	37.4	65.76	0.12	0.3	86.09	125.37
18	560	22.0	38.68	0.15	0.3	100.60	167.70
19	710	35.2	78.47	0.08	0.1	28.38	56.34
20	710	35.0	78.03	0.12	0.1	46.63	56.36
21	710	35.4	78.92	0.15	0.1	47.23	78.57
22	710	20.9	46.48	0.08	0.2	54.30	73.43
23	710	34.8	77.58	0.12	0.2	64.96	95.74
24	710	35.8	79.81	0.15	0.2	73.81	145.08
25	710	33.4	74.46	0.08	0.3	61.22	117.35
26	710	34.4	76.69	0.12	0.3	81.94	152.66
27	710	36.4	81.15	0.15	0.3	93.80	188.15

Table 2. Experimental data.

Level	n (r/min)	a_p (mm)	f (mm/r)
1	115.95	68.55	84.94
2	101.54	109.65	106.65
3	107.08	146.37	132.99
Delta	14.4	77.82	48.05
Rank	3	1	2

Table 3. Results of the range analysis of F_z .

predicting cutting forces^{13,19}. Such findings indicated that genetic algorithm could effectively search for optimal solution in multifactorial cutting experiments to find the best approaches. In this paper, GA was employed to determine the parameters of J-C constitutive model, as depicted in Fig. 6. Multiple sets of initial values for J-C constitutive parameters was firstly generated at random, then convert these values into binary encoding and input them into the fitness function derived from the least squares principle (as shown in Eq. (16)) to calculate the fitness values. Furthermore, binary encodings were chosen through a random uniform distribution, followed by crossover and mutation operations on the data to produce offspring data. This procedure was reiterated in a secondary loop until the fitness values satisfied the set criteria or the iteration count reached its maximum, culminating in the release of optimal solution.

To enhance the search velocity and precision of parameter identification using genetic algorithm, it was imperative to define logical bounds for the J-C constitutive parameters. This is crucial because different identification techniques can produce varying parameter values. In pursuit of the optimal solution for the fitness function mentioned in Fig. 6, this study collated data from extensive literature reviews, presenting constitutive parameters values, as detailed in Table 4.

From Table 4, the range of constitutive parameters can be determined as follows:

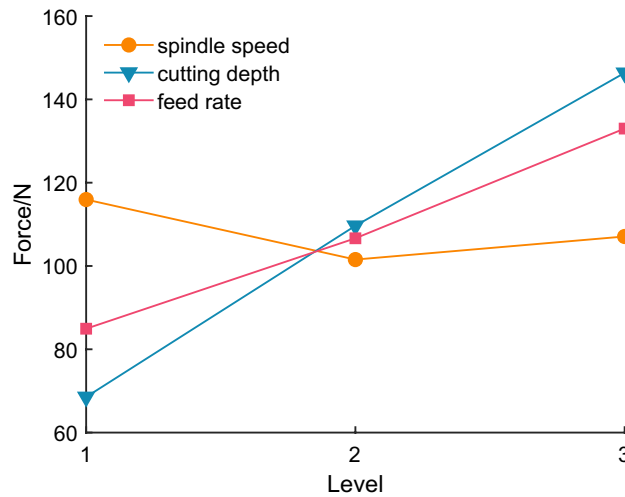


Fig. 5. The influence of experimental parameters on cutting force.

$$\begin{cases} 200 \leq A \leq 500 \\ 400 \leq B \leq 1000 \\ 0.2 \leq n \leq 0.92 \\ 0.004 \leq C \leq 0.14 \\ 0.4 \leq m \leq 1.2 \end{cases} \quad (18)$$

Initially, the genetic algorithm was used to identify the five parameters A , B , n , C , and m . However, only the value of C consistently remained at 0.14 according to the identification results, falling into a local minimum. The values of the other four parameters (A , B , n , m) would vary within a certain range, and when the five parameters obtained via the genetic algorithm were used for simulation, the simulation could not proceed normally, and the force curve could not stabilize.

Research revealed that among the five constitutive parameters A , B , n , C , and m , A and B have a significant impact on simulated cutting force, while the impact of C is minor¹³. However, after simulation tests, within the range of $0.004 \leq C \leq 0.14$, larger value of parameter C resulted in unstable simulation result and irregular chip morphology. Parameter C has the largest range of variation comparing to other four parameters (A , B , n , m) in Table 4, then it is prone to falling into local minimum in the genetic algorithm, resulting in premature termination of the simulation. Therefore, it is necessary to discuss and analyze the value of C to ensure the generation of regular chips. Since the C value of 0.0067 in the JC1 model from Table 4 is the smallest, research based on the constitutive parameters of the JC1 model was conducted. Taking the parameter $C = 0.0067$ (0%) from the JC1 model as a baseline, the values of C are set to 0.004 (-40%), 0.0054 (-20%), 0.008 (20%), 0.0094 (40%), and the maximum value of C from Table 4, which is 0.136, with a total of six levels for simulation analysis using the first set of cutting parameters (spindle speed n with 400 r/min, cutting speed v with 39.94 m/min, feed rate f with 0.08 mm/r, cutting depth with 0.1 mm) in Table 2. The resulting chip morphologies are shown in Fig. 7. Additionally, different values of the constitutive parameter C resulted in different distributions of shear zone and strain rate. As shown in Fig. 8, the shear zone and strain rate distribution results were obtained through software analysis; Along the radial center of strain rate cloud diagram in the shear zone, the strain rate and stress were extracted, and their maximum values are recorded in Table 5. Combining Fig. 7a and 8a, when C was 0.136, the maximum strain rate and stress were $58,201.29 \text{ s}^{-1}$ and 2211.28 MPa (as shown in Table 5), and no chip was produced. The reason is that the increase of C value leading to higher stress in the shear zone and elevated cutting temperatures, which surpassed the set melting point, finally preventing chip formation. As shown in Fig. 7e,f, when C were 0.008 and 0.0094, the simulation temperature remains high, hence, no complete chips were formed; by comparing the chip morphologies in Fig. 7b–d, it is observed that the most regular chips are produced when C was 0.0054, obtaining the most stable simulation. And as shown in Table 5, when C is 0.0054, the simulation force F_s (65.31 N) is closest to the experimental force F_z (62.46 N) corresponding to Table 2. Consequently, C was determined to be 0.0054, then reverse identification was utilized to obtain four remaining parameters (A , B , n , m).

($A = 452.0$, $B = 694.0$, $n = 0.311$, $m = 0.996$).

The fitness function and the constraint matrix of constitutive parameters were coded. Genetic algorithm was employed for computation via MATLAB with the following parameters: population size was 20, evolution times was 500, and algorithm tolerance is 10^{-6} . The fitness evolution trend was depicted in Fig. 9. By the time the population reached the 190th generation, it exhibited signs of stabilization and convergence. At this juncture, genetic algorithm terminated its operation. The output values for parameters A , B , n , and m were determined as the optimal solutions. Hence, the constitutive parameters for 304 stainless steel, derived from genetic algorithm, are presented in Table 6 and are designated as the JCM model.

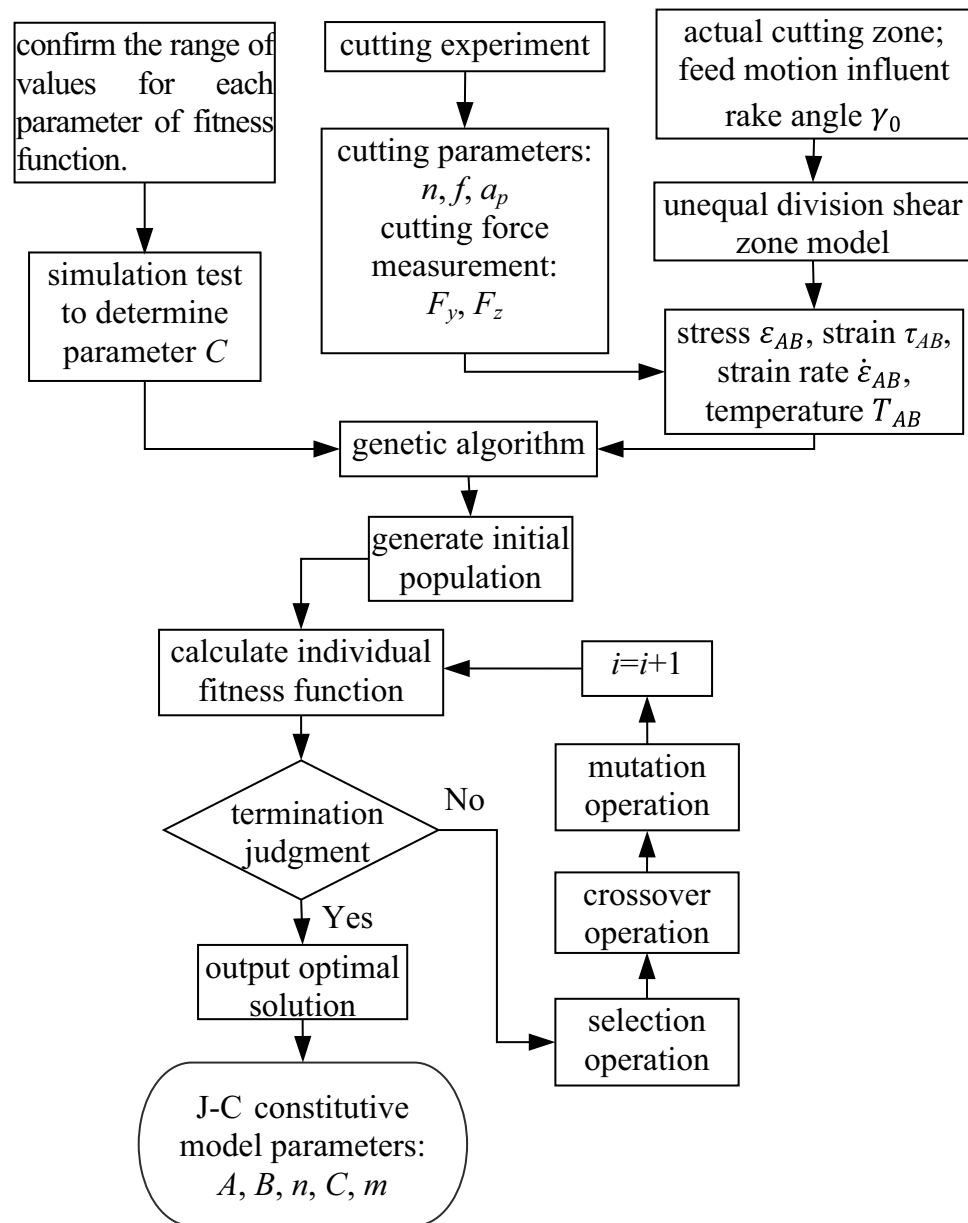


Fig. 6. Inverse identification process of constitutive parameters.

Model	A (MPa)	B (MPa)	n	C	m
JC1 ²⁶	452.0	694.0	0.311	0.0067	0.996
JC2 ¹³	357.8	801.8	0.912	0.136	0.411
JC3 ²⁷	277	556	0.796	0.0096	0.944
JC4 ²⁸	310	1000	0.65	0.07	1
JC5 ²⁹	463	426	0.25	0.015	1.03

Table 4. J-C constitutive model parameters.

FEM simulation and empirical model prediction of cutting force FEM simulation

In this study, a three-dimensional turning simulation was conducted via FEM software. Given that the workpiece diameter exceeded 20 mm, its circumferential radius was sufficiently large, thus the circular motion at the tool-workpiece contact point in Fig. 10a could be approximated as the linear motion shown in Fig. 10b. The

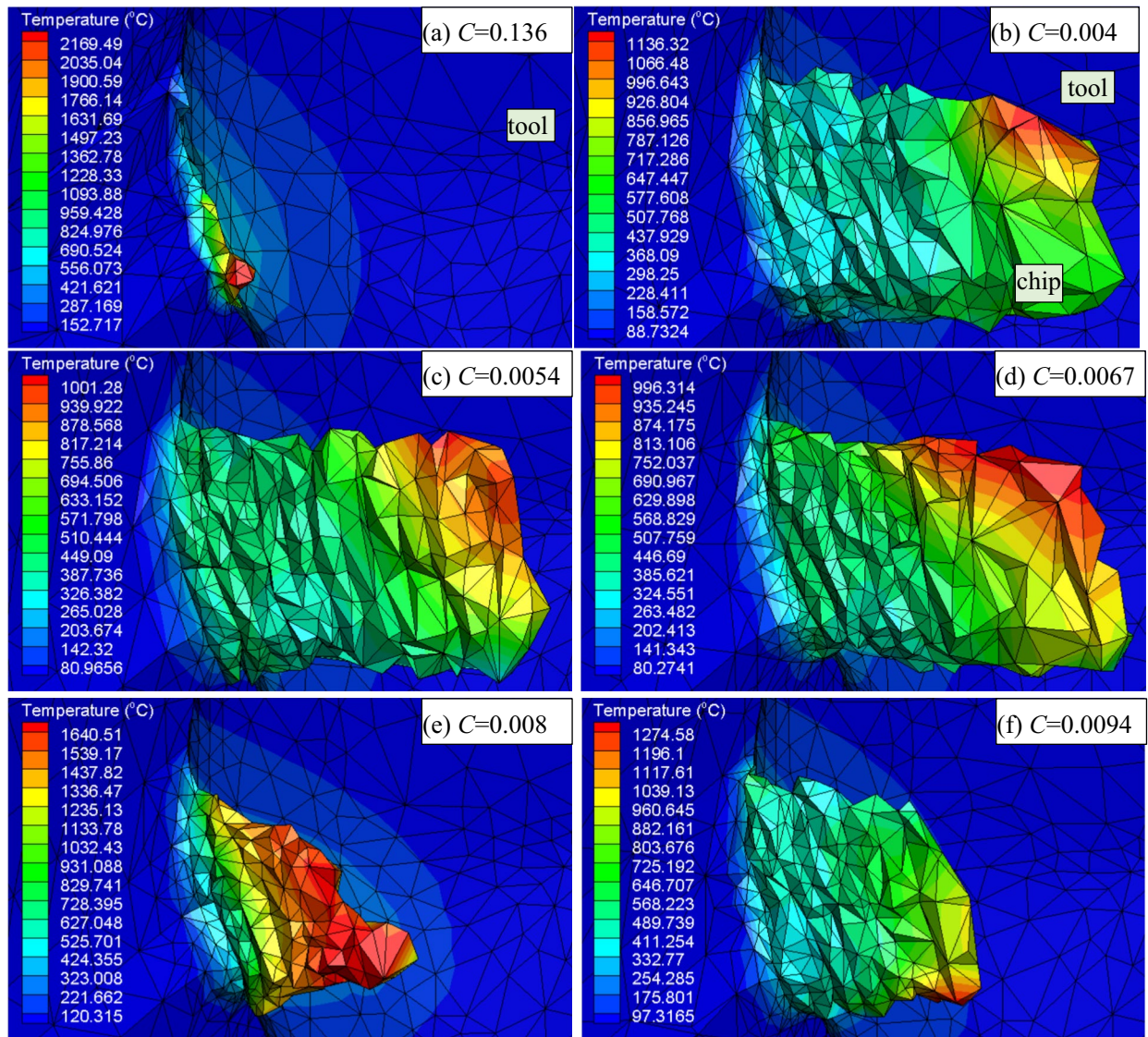


Fig. 7. Simulation results of chip morphology with different constitutive parameter C values.

designated cutting zone had dimensions of length (L) 5 mm, height (H) 2 mm, width (W) 1 mm and the tool tip model was imported. As the cutting speed cannot be fixed on an ordinary lathe, the spindle speed was selected as experimental parameter. Combined with the diameter of 304 stainless steel rod, the spindle speed was translated into cutting speed. The model mesh employed an adaptive grid, where software automatically generated a denser mesh in the cutting area and subdivided the mesh when the stress was higher. The study carried out two different simulations: Simulations based on JC1 model (as detailed in Table 4) and corresponding material parameters in literature²⁶ Simulations based on the JCM model (from genetic algorithm, as detailed in Table 6), and the material parameters presented in Table 7.

Empirical model prediction

Cutting force prediction could be implemented not only through simulation but also using empirical formulas, such as the Eq. (19)³⁰. In this study, the data of Table 2 was substituted into the Eq. (19) to conform the undetermined constants.

$$F = C_1 n^{a_1} f^{a_2} a_p^{a_3} \tag{19}$$

In the equation, C_1, a_1 to a_3 are all undetermined constants.

To linearize the nonlinear function, logarithm calculation was simultaneously executed for the both sides of Eq. (19), as shown in Eq. (20)³⁰:

$$\lg F = \lg C_1 + a_1 \lg n + a_2 \lg f + a_3 \lg a_p \tag{20}$$

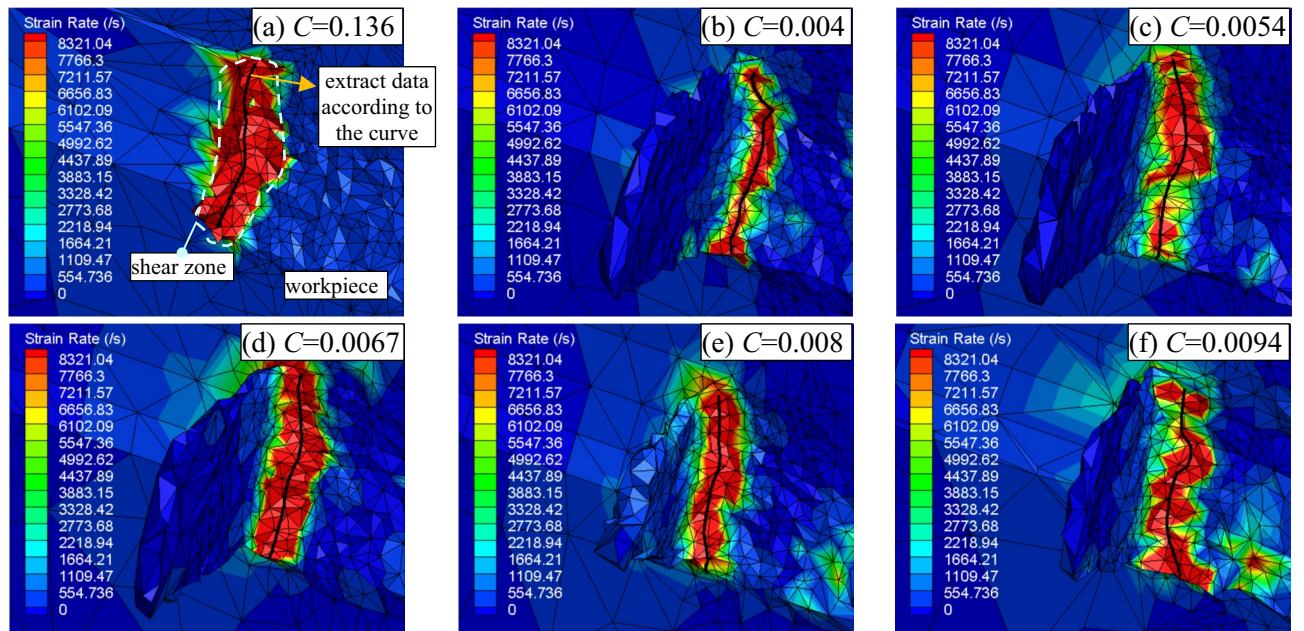


Fig. 8. Distributions of shear zone and strain rates for different values of the constitutive parameter C .

C	simulation Force F_s (N)	max strain rate (s^{-1})	max mises stress (MPa)
0.136	99.68	58,201.29	2211.28
0.004	66.57	35,024.25	899.55
0.0054	65.31	18,090.19	934.23
0.0067	74.41	31,038.75	919.68
0.008	54.55	24,050.17	961.48
0.0094	70.35	14,921.38	928.71

Table 5. The simulation force during steady state. The extracted maximum strain rate and stress.

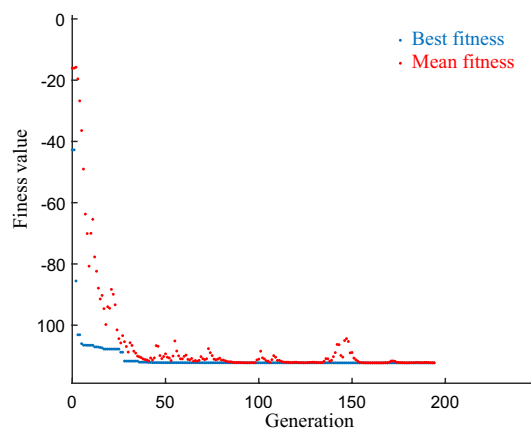


Fig. 9. Fitness trend.

A (MPa)	B (MPa)	n	C	m	$\dot{\epsilon}_0$ (s^{-1})
241.852	469.69	0.92	0.0054	1.184	0.001

Table 6. Johnson–Cook model parameters.

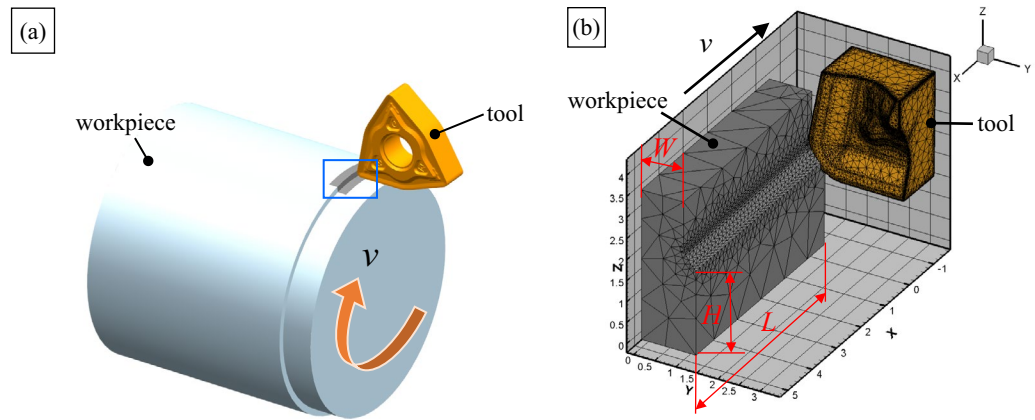


Fig. 10. The 3-D simulation model.

Density /(kg/cm ³)	Melting point /°C	Specific heat capacity /(J/kg·°C)	Elastic Modulus /Gpa	Thermal conductivity /(W/m·°C)	Poisson's ratio
7850	1400	500	210	17.3	0.33

Table 7. 304 stainless steel material parameters.

Let $b_0 = \lg c_1 + a_1 \lg n + a_2 \lg f + a_3 \lg a_p$, $x_2 = \lg f$, $x_3 = \lg a_p$. With these, the linear regression equation was obtained:

$$Y = b_0 + b_1x_1 + b_2x_2 + b_3x_3 \tag{21}$$

After executing multivariate linear regression on Eq. (21), the resultant empirical prediction model for cutting force was derived as:

$$F = 10^{3.7324} n^{-0.2055} f^{0.6899} a_p^{0.6921} \tag{22}$$

Figure 11 shows the regression residuals of prediction model. All residual data contains zero point, signifying the relative reliability of the prediction model. This empirical prediction model was referred to as EXP model. Within this model, the absolute value of corresponding exponent signifies the extent of its influence on predicted force. According to the Eq. (22), it's evident that cutting depth (0.6921) exerts the most significant influence on cutting force, followed closely by feed rate (0.6899), while spindle speed (-0.2055) exhibits the least impact.

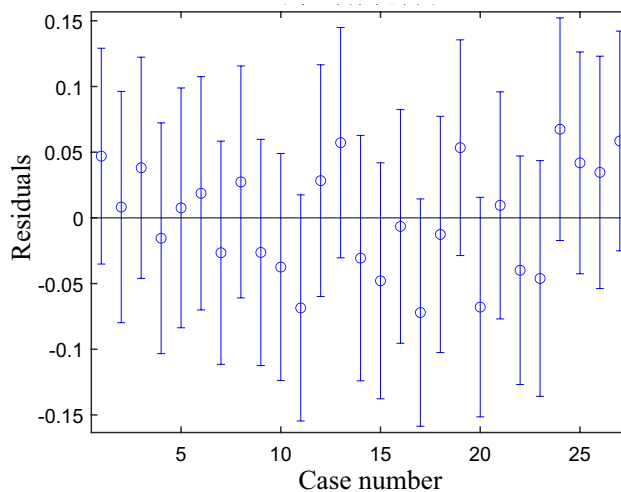


Fig. 11. Residual case order plot.

Experiment number	F^z (N)	EXP model force (N)	EXP model error (%)	JC1 model force (N)	JC1 model error (%)	JCM model force (N)	JCM model error (%)
1	62.46	56.08	10.21	70.97	13.62	67.74	8.45
2	75.57	74.18	1.83	81.48	7.83	76.01	0.59
3	94.43	86.53	8.37	104.19	10.34	92.14	2.43
4	87.39	90.61	3.68	99.30	13.63	100.32	14.80
5	121.92	119.85	1.70	131.18	7.60	122.54	0.51
6	145.89	139.80	4.18	139.90	4.10	153.55	5.25
7	112.80	119.96	6.35	127.73	13.24	123.77	9.73
8	168.92	158.68	6.06	153.07	9.38	165.42	2.07
9	174.13	185.09	6.29	167.25	3.95	179.09	2.85
10	47.99	52.33	9.05	63.41	32.13	53.19	10.84
11	59.09	69.23	17.15	89.81	51.99	66.08	11.84
12	86.15	80.75	6.27	86.11	5.52	78.67	8.67
13	96.42	84.55	12.31	94.47	2.03	104.33	8.20
14	104.18	111.85	7.36	125.51	20.48	110.17	5.76
15	116.78	130.46	11.72	137.18	17.47	120.17	2.90
16	110.23	111.95	1.56	130.45	18.34	120.24	9.09
17	125.37	148.08	18.11	163.58	30.48	131.67	5.02
18	167.70	172.72	2.99	181.75	8.38	173.99	3.75
19	56.34	49.84	11.54	63.42	12.56	55.48	1.54
20	56.36	65.93	16.98	87.64	55.51	62.10	10.18
21	78.57	76.90	2.12	97.11	23.59	85.17	8.40
22	73.43	80.53	9.67	91.25	24.27	83.80	14.12
23	95.74	106.52	11.26	118.01	23.26	106.47	11.20
24	145.08	124.25	14.36	128.00	11.77	141.69	2.33
25	117.35	106.62	9.15	118.09	3.68	108.13	7.86
26	152.66	141.03	7.62	169.82	11.24	157.17	2.95
27	188.15	164.50	12.57	165.98	11.78	189.75	0.85
Average			8.54		16.60		6.38

Table 8. Comparison of experimental and simulated predicted results.

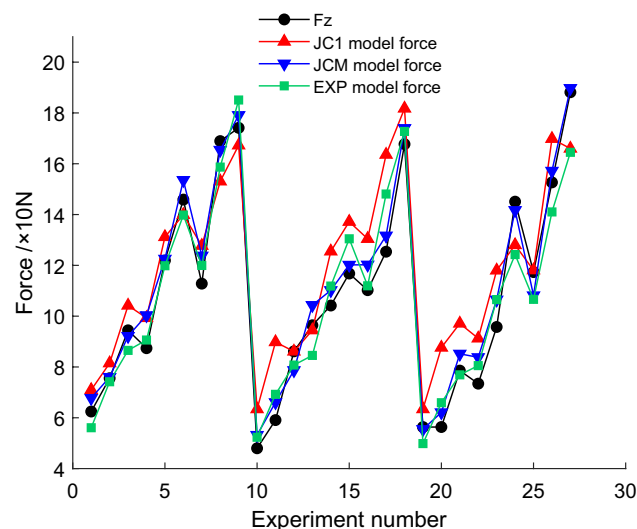


Fig. 12. Cutting force graph.

As shown in Table 8, the cutting force errors between each model value and its experimental value were calculated. Based on Table 8, a cutting force graph was depicted in Fig. 12 and an error graph was shown in Fig. 13. In JC1 model, the average error of cutting force was 16.60%, with a minimum value of 2.03% and a maximum value of 55.51%. The JC1 model exhibits a large mean error and fluctuation range (50%). This is attributed to the fact that the J-C constitutive parameters obtained from the SHPB test are just applicable within a strain rate

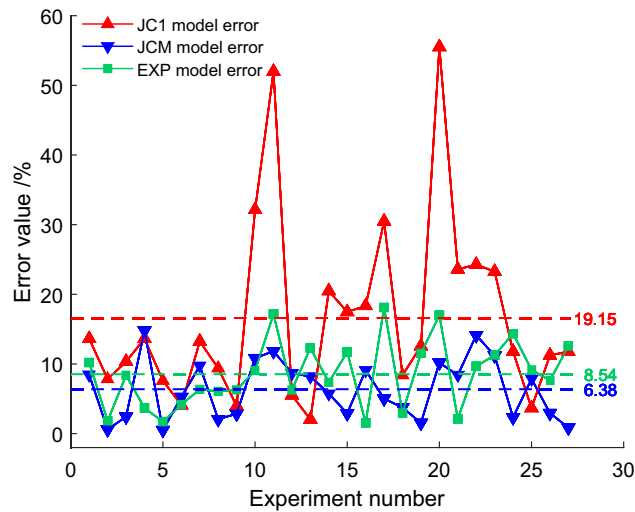


Fig. 13. Error graph.

range of $10^3 \text{ s}^{-1} \sim 10^4 \text{ s}^{-1}$. However, under turning conditions, the material's strain rate can reach 10^5 s^{-1} . Therefore, the JC1 model could not accurately reflect actual turning experiment situation. The EXP model reported an average error of 8.54%, with values spanning from 1.56% at the lowest to 18.11% at the highest. Its error fluctuation was relatively small, however, as shown in Table 8, the predicted force F_z reached its maximum value of 185.09 N in the 9th group ($n = 400 \text{ r/min}$, $f = 0.15 \text{ mm/r}$, $a_p = 0.3 \text{ mm}$), which is inconsistent with the trend of the experimental values of cutting force. While JCM model, identified through genetic algorithm, showed an average error of 6.38%, with its values fluctuating between 0.51% and 14.80%. The error range, maximum value, and average value of cutting force in JCM model were all smaller than those of EXP model, generally speaking, the error fluctuation of this model was the smallest. In this study, compared to EXP model, JCM model not only more precisely depicted the changes of actual experimental cutting force, but also coincided with actual cutting force better. It should be noted that EXP model was predicated via only three parameters—spindle speed n , feed rate f , and cutting depth a_p . While JCM model encompasses more factors of cutting process, such as the variations of cutting zone, feed motion, changes of workpiece diameter, etc.

Conclusion

1. Parameter optimization of Johnson–Cook (J-C) constitutive model for 304 stainless steel was realized by utilizing the characteristics of genetic algorithm that could efficiently obtain the optimal solutions. It could accurately reflect the state of turning machining under high strain rate conditions. The simulated values of cutting force aligned closely with its experimental values, exhibiting minimal deviation and maintaining the same trend of value changes.
2. Considering the influence of actual cutting zone and the impact of feed motion on the rake (flank) angle, an unequal division shear zone model was established in the construction process of J-C constitutive model. FEM simulation results implied that, if other parameters were held constant, the increase of C value would lead to greater stress in the shear zone and thicker chip layer that accumulated at the tool tip, causing temperature increase, resulting in the instability of cutting force.
3. Range analysis was implemented for turning experimental data, comparing the Delta and Rnak values, it was discerned that both cutting depth and feed rate had a positive correlation with cutting force. However, within the range of 400 ~ 710 r/min, spindle speed initially exhibited a negative correlation and later indicated a positive correlation with cutting force, due to the diminishing workpiece diameter which caused a decrease in cutting speed and an increase in rake angle.
4. In JC1 model, the maximum error between simulated and experimental cutting forces was 55.51%, with an average error of 16.60%. This large fluctuation in error indicated that the STN model could not accurately reflect actual turning experiment conditions. EXP model was derived through multiple linear regression, its maximum error between predicted and experimental values was 18.11%, with an average error of 6.38%. Moreover, the predicted values of cutting force failed to consistently align with experimental results. The range of cutting forces simulated by JCM model was 53.19 ~ 189.75 N. The maximum error between experimental value and simulated value was 14.8%, with an average error of 6.38%. These results demonstrated that JCM model suited the actual experiments conducted in this study the most.
5. It was evident that the error range and average values of JCM model identified in this paper were superior to those of JC1 and EXP models. It suggested that JCM model could accurately capture the variations of cutting force for 304 stainless steel workpieces with different diameters, especially at low to medium spindle speeds. The feasibility of reverse identification method based on genetic algorithm and the reliability as well as accuracy of J-C constitutive model were also verified.

Data availability

The datasets used and/or analysed during the current study are available from the corresponding author on reasonable request. Correspondence and requests for materials should be addressed to C.W.

Received: 20 May 2024; Accepted: 29 August 2024

Published online: 11 September 2024

References

1. Wang, H., Chen, L., Liu, D., Song, G. & Tang, G. Study on electropulsing assisted turning process for AISI 304 stainless steel. *Mater. Sci. Technol.* **31**, 1564–1571 (2015).
2. Zahrani, E. G., Azarhoushang, B. & Wilde, J. Evaluation of chip breaking in combined laser-turning process. *J. Manufact. Process.* **77**, 722–729 (2022).
3. Ahmed, Y. S., Paiva, J. M. & Veldhuis, S. C. Characterization and prediction of chip formation dynamics in machining austenitic stainless steel through supply of a high-pressure coolant. *Int. J. Adv. Manuf. Technol.* **102**, 1671–1688 (2019).
4. Du, H., Karasev, A., Bjork, T., Loyquist, S. & Jonsson, P. G. Assessment of Chip Breakability during Turning of Stainless Steels Based on Weight Distributions of Chips. *Metals* **10**, 675 (2020).
5. Xu, Y., Wan, Z., Zou, P. & Zhang, Q. Experimental study on chip shape in ultrasonic vibration-assisted turning of 304 austenitic stainless steel. *Adv. Mech. Eng.* **11**, 1–17 (2019).
6. Oxley, P. A mechanics of machining approach to assessing machinability. In *Proceedings twenty-second international machine tool design and research conference* (ed. Oxley, P.) (Springer, 1982).
7. Astakhov, V. P., Osman, M. O. M. & Hayajneh, M. T. Re-evaluation of the basic mechanics of orthogonal metal cutting: velocity diagram, virtual work equation and upper-bound theorem. *Int. J. Mach. Tools Manufact.* **41**, 393–418 (2001).
8. Tounsi, N., Vincenti, J., Otho, A. & Elbestawi, M. A. From the basic mechanics of orthogonal metal cutting toward the identification of the constitutive equation. *Int. J. Mach. Tools Manufact.* **42**, 1373–1383 (2002).
9. Zhou, F., Wang, X., Hu, Y. & Ling, L. Modeling temperature of non-equidistant primary shear zone in metal cutting. *Int. J. Therm. Sci.* **73**, 38–45 (2013).
10. Bodner, S. R. & Partom, Y. Constitutive equations for elastic-Viscoplastic strain-hardening materials. *J. Appl. Mech.* **42**, 385–389 (1975).
11. Johnson, G. R. & Cook, W. H. Fracture characteristics of three metals subjected to various strains, strain rates, temperatures and pressures. *Eng. Fract. Mech.* **21**, 31–48 (1985).
12. Zerilli, F. J. & Armstrong, R. W. Dislocation-mechanics-based constitutive relations for material dynamics calculations. *J. Appl. Phys.* **61**, 1816–1825 (1987).
13. Zou, Z. *et al.* Research on inverse identification of johnson-cook constitutive parameters for turning 304 stainless steel based on coupling simulation. *J. Mater. Res. Technol.-JMRT* **23**, 2244–2262 (2023).
14. Hou, Q. Y. & Wang, J. T. A modified Johnson-Cook constitutive model for Mg–Gd–Y alloy extended to a wide range of temperatures. *Comput. Mater. Sci.* **50**, 147–152 (2010).
15. Meng, X., Lin, Y. & Mi, S. An improved Johnson-cook constitutive model and its experiment validation on cutting force of ADC12 aluminum alloy during high-speed milling. *Metals* **10**, 1038 (2020).
16. Chen, X., Wang, X., Xie, L., Wang, T. & Ma, B. Determining Al6063 constitutive model for cutting simulation by inverse identification method. *Int. J. Adv. Manuf. Technol.* **98**, 47–54 (2018).
17. Shen, X., Zhang, D., Yao, C., Tan, L. & Li, X. Research on parameter identification of Johnson-Cook constitutive model for TC17 titanium alloy cutting simulation. *Mater. Today Commun.* **31**, 103772 (2022).
18. Nguyen, N. & Hosseini, A. Direct calculation of Johnson-Cook constitutive material parameters for oblique cutting operations. *J. Manufact. Process.* **92**, 226–237 (2023).
19. Zhou, T. *et al.* Inverse identification of material constitutive parameters based on co-simulation. *J. Mater. Res. Technol.* **20**, 221–237 (2022).
20. Yao, D., Duan, Y., Li, M. & Guan, Y. Hybrid identification method of coupled viscoplastic-damage constitutive parameters based on BP neural network and genetic algorithm. *Eng. Fract. Mech.* **257**, 108027 (2021).
21. Li, B. & Zhang, R. Analytical prediction of cutting forces in cylindrical turning of 304 stainless steel using unequal division shear zone theory. *Int. J. Adv. Manuf. Technol.* **124**, 3201–3215 (2023).
22. Fu, Z., Yang, W., Wang, X. & Leopold, J. Analytical modelling of milling forces for helical end milling based on a predictive machining theory. *Proc. CIRP* **31**, 258–263 (2015).
23. Lalwani, D. I., Mehta, N. K. & Jain, P. K. Extension of Oxley's predictive machining theory for Johnson and Cook flow stress model. *J. Mater. Process. Technol.* **209**, 5305–5312 (2009).
24. Li, B., Wang, X., Hu, Y. & Li, C. Analytical prediction of cutting forces in orthogonal cutting using unequal division shear-zone model. *Int. J. Adv. Manuf. Technol.* **54**, 431–443 (2011).
25. Johnson, G. R. & Cook, W. A Constitutive Model And Data For Metals Subjected To Large Strains, High Strain Rates And High Temperatures. (2018).
26. Zhang, W., Wang, X., Hu, Y. & Wang, S. Predictive modelling of microstructure changes, micro-hardness and residual stress in machining of 304 austenitic stainless steel. *Int. J. Mach. Tools Manufact.* **130–131**, 36–48 (2018).
27. Ling, L., Li, X., Wang, X. & Hu, Y. Constitutive model of stainless steel 0Cr18Ni9 and Its influence on cutting force prediction. *China Mech. Eng.* **23**, 2243–2248 (2012).
28. Laakso, S. V. A., Agmell, M. & Ståhl, J.-E. The mystery of missing feed force—The effect of friction models, flank wear and ploughing on feed force in metal cutting simulations. *J. Manufact. Process.* **33**, 268–277 (2018).
29. Li, J. C., Chen, X. W. & Huang, F. L. FEM analysis on the deformation and failure of fiber reinforced metallic glass matrix composite. *Mater. Sci. Eng. A* **652**, 145–166 (2016).
30. Xu, C. *et al.* Experimental tests and empirical models of the cutting force and surface roughness when cutting 1Cr13 martensitic stainless steel with a coated carbide tool. *Adv. Mech. Eng.* **8**, 1687814016673753 (2016).

Acknowledgements

This work was supported by the National Key R&D Program of China (No. 2018YFE0199100), the Joint Fund of Zhejiang Provincial Natural Science Foundation of China under Grant No. LZYZ3E050003 and LZYZ3E050002, and Public Welfare Project of Zhejiang Province (No.LGG22F030013). The authors also sincerely appreciate the technical support from the optical 3D surface profilometer (CHOTEST SuperView W1).

Author contributions

X.J., J.D. and C.W. proposed the concept of the paper, designed the experiments and wrote the main manuscript text. X.J. prepared Figs. 1–13. S.E., L.H. and W.Y. assisted in the experiment. H.W., C.Z. and W.Y. contributed in data analysis. All authors reviewed the manuscript.

Competing interests

The authors declare no competing interests.

Additional information

Correspondence and requests for materials should be addressed to C.W. or L.H.

Reprints and permissions information is available at www.nature.com/reprints.

Publisher's note Springer Nature remains neutral with regard to jurisdictional claims in published maps and institutional affiliations.

Open Access This article is licensed under a Creative Commons Attribution-NonCommercial-NoDerivatives 4.0 International License, which permits any non-commercial use, sharing, distribution and reproduction in any medium or format, as long as you give appropriate credit to the original author(s) and the source, provide a link to the Creative Commons licence, and indicate if you modified the licensed material. You do not have permission under this licence to share adapted material derived from this article or parts of it. The images or other third party material in this article are included in the article's Creative Commons licence, unless indicated otherwise in a credit line to the material. If material is not included in the article's Creative Commons licence and your intended use is not permitted by statutory regulation or exceeds the permitted use, you will need to obtain permission directly from the copyright holder. To view a copy of this licence, visit <http://creativecommons.org/licenses/by-nc-nd/4.0/>.

© The Author(s) 2024